Elsevier Editorial System(tm) for Materials Science and Engineering C
Manuscript Draft

Manuscript Number: MSEC-D-14-00687R1

Title: Cannabinoid antagonist in nanostructured lipid carriers (NLC): design, characterization and in vivo study

Article Type: Research Paper

Keywords: Nanostructured lipid carriers; rimonabant; cryogenic transmission electron microscopy; photon correlation spectroscopy; drug delivery

Corresponding Author: Prof. Claudio Nastruzzi,

Corresponding Author's Institution: University of Ferrara

First Author: Elisabetta Esposito

Order of Authors: Elisabetta Esposito; Laura Ravani; Markus Drechsler; Paolo Mariani; Catia Contado; Janne Ruokolainen; Patrizia Ratano; Patrizia Campolongo; Viviana Trezza; Claudio Nastruzzi; Rita Cortesi

Abstract: This study describes the preparation, characterization, and in vivo evaluation in rats of nanostructured lipid carriers (NLC) encapsulating rimonabant (RMN) as prototypical cannabinoid antagonist.A study was conducted in order to optimize NLC production by melt and ultrasonication method. NLC were prepared by alternatively adding the lipid phase into the aqueous one (direct protocol) or the aqueous phase into the lipid one (reverse protocol). RMN-NLC have been characterized by Cryogenic Transmission Electron Microscopy (cryo-TEM), x-ray, Photon Correlation Spectroscopy (PCS) and Sedimentation Field Flow Fractionation (SdFFF). Reverse NLC were treated with polysorbate 80. RMN release kinetics have been determined in vitro by dialysis method. In vivo RMN biodistribution in rats was evaluated after intranasal (i.n.) administration of reverse RMN-NLC.The reverse protocol enabled to prevent the lost of lipid phase and to achieve higher RMN encapsulation efficacy (EE) with respect to the direct protocol (98 % w/w versus 67% w/w).The use of different protocols did not affect NLC morphology and dimensional distribution.An in vitro dissolutive release rate of RMN was calculated. The in vivo data indicate that i.n. administration of RMN by reverse NLC treated with polysorbate 80 increased RMN concentration in the brain with respect to the drug in solution.The nanoencapsulation protocol presented here appears as an optimal strategy to improve the low solubility of cannabinoid compounds in an aqueous system suitable for in vivo administration.

Cover Letter

Ferrara, 3 june 2014

Dear Editor in Chief,

Enclosed please find a manuscript to be submitted for possible publication on “Materials Sciences and Engineering C”.
The manuscript is entitled:
“Cannabinoid antagonist in nanostructured lipid carriers (NLC): design, characterization and in vivo study"
by Elisabetta Esposito, Laura Ravani, Markus Drechsler, Paolo Mariani, Catia Contado, Patrizia Ratano, Patrizia Campolongo, Viviana Trezza, Claudio Nastruzzi and Rita Cortesi.

The manuscript regards a nanoencapsulation strategy able to improve the solubility of cannabinoid compounds in an aqueous system suitable for in vivo administration. Interestingly, the intranasal administration of nanoparticles allows to increase cannabinoid concentration in the brain with respect to the drug in solution.

The manuscript is original, unpublished, it is not under consideration for publication elsewhere, and all authors have read and approved the text and consent to its publication.

I thank you in advance for consideration.
Best regards
Prof Claudio Nastruzzi

We thank the Editor and the Reviewers for their positive and insightful comments on our manuscript. We have revised the manuscript to accomplish with the Reviewers' suggestions. Essentially, we have performed DSC analyses and inserted a new Figure. Results and Discussion have been improved with new comments, accordingly three new references have been added.

In reply to Reviewer #1

1.Page no 24 Table III title does not appears

The title of the Table reported in the Bottom of Figure 5 (now Figure 6) has been inserted.

2. Authors not discussed quantity of rimonabant added during NLC preparation.

The quantity of RMN added during NLC preparation has been discussed in the "Result " section of the revised manuscript (pag 14).

2. How dose of rimonabant for nasal administration is selected?

The dose of Rimonabant for intranasal administration has been selected on the basis of our own previous studies and literature data. In particular, we administered a dose of the drug that has been proven to antagonize the effects of cannabinoid receptor agonists on different behavioral endpoints, without inducing effects by its own (Bosier et al., Neuropharmacology 59 (2010) 503-510; Bortolato et al., Neuropsychopharmacology.2006 Dec;31(12):2652-9, Campolongo et al., Psychopharmacology (Berl). 2011 Mar;214(1):5-15).
This information has now been added in the method section of the revised manuscript. Accordingly three new references (31-34) have been added.

3. NLC formulation contains lipids material thermal analysis is need to be studied.

In order to accomplish with the reviewer's suggestion, differential scanning calorimetry (DSC) analyses have been conducted. In particular NLC, RMN-NLC and the fused lipid mixture in the absence and in the presence of RMN have been analyzed.

Accordingly, the employed DSC method, Figure 5 and the result have been added.

We wish that now the manuscript could be acceptable for publication

Best regards

***Suggest Reviewers**

K Mackie

e-mail: kmackie@u.washington.edu

K. Mackie is an expert in cannabinoids and their therapeutic uses

Agnieszka Z. Wilczewska

e-mail: agawilcz@uwb.edu.pl

A. Z. Wilczewska is an expert in nanoparticles

Sanjeeb K. Sahoo

e-mail: sanjeebsahoo2005@gmail.com

Sanjeeb K. Sahoo is an expert in nanoparticles

Graphical Abstract (for review)

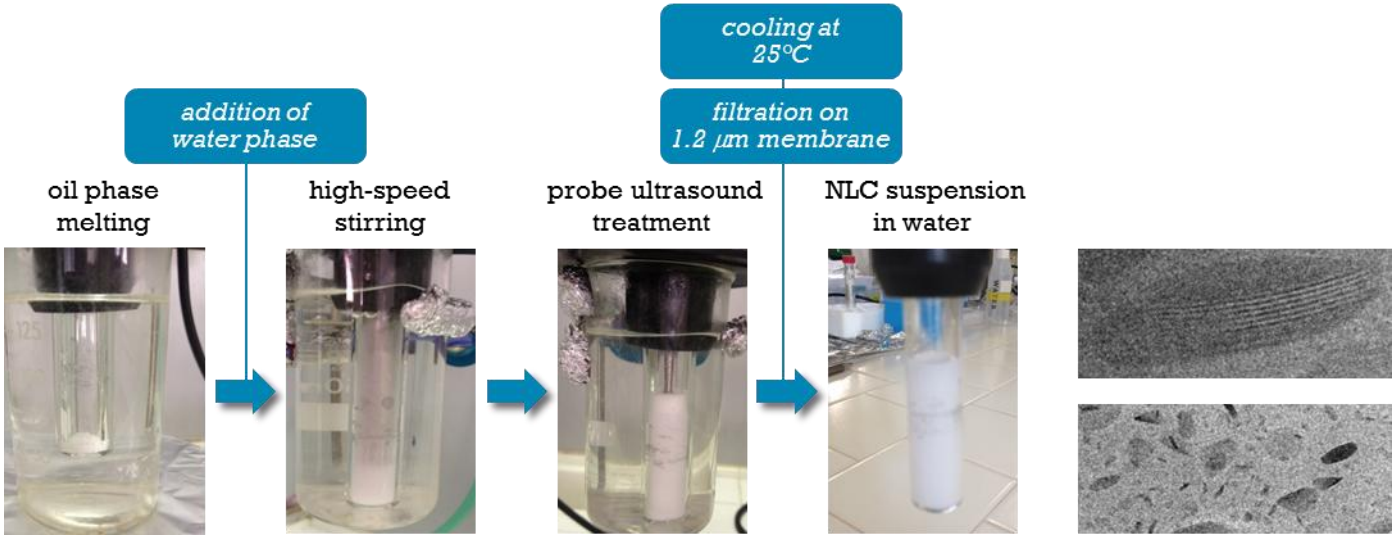

***Highlights (for review)**

-Rimonabant (RMN) can be encapsulated in nanostructured lipid carriers (NLC)

-Nanoencapsulation improves RMN solubility in a stable physiologic aqueous formulation

- RMN is released in vitro from NLC by a controlled dissolutive release modality

- I.n. administration leads to higher RMN concentration in brain with respect to plasma

- NLC increases RMN concentration in the brain with respect to reference solution of RMN

Cannabinoid antagonist in nanostructured lipid carriers (NLC): design, characterization and in vivo study

Running title: Rimonabant delivered by nanostructured lipid carriers

Elisabetta Esposito[a], Laura Ravani[a], Markus Drechsler[b], Paolo Mariani[c], Catia Contado[d], Janne Ruokolainen[e], Patrizia Ratano[f], Patrizia Campolongo[f], Viviana Trezza[g], Claudio Nastruzzi[a*], Rita Cortesi[a]

[a]*Department of Life Sciences and Biotechnology, University of Ferrara, I-44121 Ferrara, Italy*
[b]*BIMF / Soft Matter Electronmicroscopy , University of Bayreuth, Germany*
[c]*Department of Life and Environmental Sciences and CNISM, Università Politecnica delle Marche, I-60100 Ancona, Italy*
[d]*Department of Chemistry, University of Ferrara, I-44121 Ferrara, Italy*
[e]*Department of Applied Physics, Aalto University, 00076- Aalto, Finland*
[f]*Department of Physiology and Pharmacology, Sapienza University of Rome, 00185 Roma, Italy*
[g]*Department of Science, Roma Tre University, 00146 Roma, Italy*

[*]Correspondence to:
Prof Claudio Nastruzzi
Department of Life Sciences and Biotechnology
Via Fossato di Mortara, 19
I-44121 Ferrara, Italy
Tel. +39/0532/455348
Fax. +39/0532/455953
e-mail nas@unife.it

ABSTRACT

This study describes the preparation, characterization, and in vivo evaluation in rats of nanostructured lipid carriers (NLC) encapsulating rimonabant (RMN) as prototypical cannabinoid antagonist.

A study was conducted in order to optimize NLC production by melt and ultrasonication method. NLC were prepared by alternatively adding the lipid phase into the aqueous one (direct protocol) or the aqueous phase into the lipid one (reverse protocol). RMN-NLC have been characterized by Cryogenic Transmission Electron Microscopy (cryo-TEM), x-ray, Photon Correlation Spectroscopy (PCS) and Sedimentation Field Flow Fractionation (SdFFF). Reverse NLC were treated with polysorbate 80. RMN release kinetics have been determined in vitro by dialysis method. In vivo RMN biodistribution in rats was evaluated after intranasal (i.n.) administration of reverse RMN-NLC.

The reverse protocol enabled to prevent the lost of lipid phase and to achieve higher RMN encapsulation efficacy (EE) with respect to the direct protocol (98 % w/w versus 67% w/w).

The use of different protocols did not affect NLC morphology and dimensional distribution.

An in vitro dissolutive release rate of RMN was calculated. The in vivo data indicate that i.n. administration of RMN by reverse NLC treated with polysorbate 80 increased RMN concentration in the brain with respect to the drug in solution.

The nanoencapsulation protocol presented here appears as an optimal strategy to improve the low solubility of cannabinoid compounds in an aqueous system suitable for in vivo administration.

Keywords: Nanostructured lipid carriers; rimonabant; cryogenic transmission electron microscopy; photon correlation spectroscopy; drug delivery

Abbreviations: Nanostructured lipid carriers: NLC; rimonabant: RMN, cryogenic transmission electron microscopy: cryo-TEM; photon correlation spectroscopy: PCS; Sedimentation Field Flow Fractionation: SdFFF; oil phase in water phase method: direct method; water phase in oil phase method: reverse method.

INTRODUCTION

Since the identification of cannabinoid receptors and their endogenous lipid ligands, the endocannabinoid system and its regulatory functions in health and disease have been object of a large number of studies. For instance, it has been demonstrated that the administration of cannabinoid compounds affects a number of physiological functions, both in the central and peripheral nervous systems and in peripheral organs (1, 2).

In this respect, the pharmacological manipulation of the endocannabinoid signaling could represent a therapeutic opportunity to treat many diseases and pathological conditions, spanning from, movement disorders (i.e. Parkinson's and Huntington's diseases), cognitive dysfunction, anxiety disorders, social disabilities, alcohol addiction, neuropathic pain, multiple sclerosis and spinal cord injury, to cancer, atherosclerosis, myocardial infarction, stroke, hypertension, glaucoma and obesity/metabolic syndrome (3-8).

Many preclinical studies and clinical trials with compounds able to modulate the endocannabinoid system are in progress, possibly resulting in novel or ameliorated therapeutic approaches (9, 10). Nevertheless it should be considered that due to the scarce solubility of cannabinoids drugs in aqueous media, their handling and dosing is arduous. This difficulty in administering cannabinoids drugs in an efficient way not only restricts their use in medicines but also limits their preclinical investigations in animal models, requiring the use of non-aqueous solution or unstable suspensions (11).

In order to solubilize cannabinoid drugs in a physiologic stable medium and possibly to improve their brain target, a nanoparticulate system appears as the optimal solution.

Lipid-based nanoparticles can be considered as a versatile tool with a high potential of applications; in fact they can solubilize a number of molecules with different chemico-physical properties in a biocompatible and biodegradable matrix with well-established

safety profiles (12, 13). The matrix of solid lipid nanoparticles (SLN) can improve the stability of labile molecules, improving their bioavailability and assuring restrained release profile (14, 15).

A particular kind of SLN is typified by nanostructured lipid carriers (NLC), whose components are lipids in solid state at room and body temperatures, mixed with lipids in liquid state (16). Production of NLC by blends of lipids results in the formation of an imperfect and disordered lipid matrix which can accommodate poor soluble drugs (17). Given their characteristics, NLC can be considered as preferable nanovectors with respect to SLN since they can increase drug loading and longer assure molecule stability (18). Moreover NLC maintain their physical stability for long periods of time (usually more than 1 year) and can be administered by different routes, including oral to intranasal, achieving prolonged therapeutic blood levels for the included drug (19).

The goal of this study was the design and production of NLC containing cannabinoid drugs. To this aim rimonabant (RMN) was employed as model cannabinoid antagonist in reason of its physico-chemical characteristics that are very similar to many other cannabinoid molecules (20, 21).

Particularly, alternative production strategies have been investigated and the influence of the various experimental protocols on NLC morphology, dimensional distribution and inner structure has been investigated by mean of Cryogenic Transmission Electron Microscopy (cryo-TEM), Photon Correlation Spectroscopy (PCS), x-ray and Sedimentation Field Flow Fractionation (SdFFF) (22). Moreover RMN release kinetics from NLC were studied by in vitro experiments.

Finally a preliminary in vivo study has been performed in rats administering RMN-NLC by intranasal (i.n.) route and measuring plasma and brain RMN concentration 6 hours after administration.

MATERIALS AND METHODS

Materials

The copolymer poly (ethylene oxide) (PEO, a) –poly (propylene oxide) (PPO, b) (a=80, b=27) (poloxamer 188) was a gift of BASF ChemTrade GmbH (Burgbernheim, Germany). Tristearin, stearic triglyceride (tristearin) and polysorbate 80 were provided by Fluka (Buchs-Swiss). Miglyol 812 N, caprylic/capric triglycerides (miglyol) was a gift of Cremer Oleo Division (Witten, Germany). All other chemicals were from Sigma-Aldrich (Milano, Italy). The cannabinoid antagonist SR1417165; (4-Chlorophenyl)-1-(2,4-dichloro-phenyl)-4-methyl-N-(piperidin-1-yl)-1H-pyrazole-3-carboxamide (rimonabant) was a kind gift of RTI International, Durham, NC, USA.

Preformulation study

NLC were prepared by melt and ultrasonication method (23). Briefly, 0.25 g of lipid mixture was melted at 80°C. The lipid mixture was constituted of tristearin/miglyol 2:1 w/w. NLC were obtained by two alternative approaches, depending on the mixing modality of oil phase (OP) and water phase (WP), adopted to form the O/W emulsion that constitutes the crucial step for the preparation of the NLC. In one case, named "direct method" the melted OP is added to the WP, while in the other, named "reverse method" the WP is added to the OP.

Direct method

The OP was molten in a beaker and then poured in a vial containing 4.75 ml of an aqueous poloxamer 188 solution (WP) (2.5 % w/w) heated at 80°C. The mixture was then emulsified at 15000 rpm, 80°C for 1 min, using a high-speed stirrer (Ultra Turrax T25, IKA-Werke GmbH & Co. KG, Staufen, Germany). The emulsion was subjected to

ultrasonication (Microson TM, Ultrasonic cell Disruptor) at 6.75 kHz for 15 min and then cooled down to room temperature by placing it in a water bath at 25 °C.

Reverse method

NLC were prepared by pouring the WP (80°C) into the vial containing the molten OP. The mixture was then emulsified with the same modalities above reported (stirring at 15000 rpm, 80°C for 1 min, followed by ultrasonication at 6.75 kHz for 15 min). In the case of RMN containing NLC (RMN-NLC), produced by the "direct" or the "reverse" methods, RMN (0.2% w/w with respect to total weight of dispersion) was added to the lipid mixture and dissolved before addition to the aqueous solution. The emulsion was then cooled down to room temperature by placing it in a water bath at 25 °C. After cooling, empty NLC and RMN-NLC were filtered through a mixed esters cellulose membrane (1.2 μm pore size) in order to remove the possibly presence of lipid aggregates. All glassware and filter employed for the NLC production were accurately weighted before and after preparation of NLC. The NLC dispersions were stored at room temperature. In the case of NLC prepared by "reverse method", polysorbate 1% w/w was added to the dispersion after ultrasonication and left under stirring (250 rpm) for 30 min.

Characterization of NLC

Cryo-TEM analysis

Samples were vitrified as described in a previous study by Esposito et al. (23). The vitrified specimen was transferred to a Zeiss EM922Omega transmission electron microscope for imaging using a cryoholder (CT3500, Gatan). The temperature of the sample was kept below -175 °C throughout the examination. Specimens were examined with doses of about 1000-2000 e/nm^2 at 200 kV. Images were recorded digitally by a CCD camera (Ultrascan 1000, Gatan) using an image processing system (GMS 1.9 software, Gatan).

X-ray diffraction measurements

X-ray diffraction experiments were performed using a 3.5 kW Philips PW 1830 X-ray generator (Amsterdam, Netherlands) equipped with a Guinier-type focusing camera (homemade design and construction, Ancona, Italy) operating with a bent quartz crystal monochromator (λ= 1.54 Å). Diffraction patterns were recorded on GNR Analytical Instruments Imaging Plate system (Novara, Italy). Samples were held in a tight vacuum cylindrical cell provided with thin mylar windows. Diffraction data were collected at 37° and 45°C. In each experiment, a number of Bragg peaks was detected in the low-angle region and the peak indexing was performed considering the different symmetries commonly observed in lipidic phases (24). Once derived the lattice symmetry, the unit cell dimension, a, was calculated from the averaged spacing of the observed peaks.

Photon Correlation Spectroscopy (PCS)

Submicron particle size analysis was performed using a Zetasizer 3000 PCS (Malvern Instr., Malvern, England) equipped with a 5 mW helium neon laser with a wavelength output of 633 nm. Glassware was cleaned of dust by washing with detergent and rinsing twice with water for injections. Measurements were made at 25 °C at an angle of 90°. Data were interpreted using the “method of cumulants” (25).

Sedimentation Field Flow Fractionation Analysis

A sedimentation field flow fractionation analysis (SdFFF) system (Model S101, FFFractionation, Inc., Salt Lake City, UT, USA), described elsewhere (26), was employed to determine the size distribution of particles by converting the fractograms, i.e. the graphical results, assuming that the particle density is known (27). The mobile phase was

demineralized water pumped at 2.0 ml/min and monitored in each run. Fifty microliter samples were injected as they were through a 50 µl Rheodyne loop valve. The fractions were automatically collected after the SdFFF system by a Model 2110 fraction collector (Bio Rad laboratories, UK) with a collecting time of 90 sec. The volume of each fraction was 3 ml.

Differential scanning calorimetry

Differential scanning calorimetry (DSC) measurements of NLC, RMN-NLC, the bulk mixture of tristearin and miglyol or the bulk mixture of tristearin and miglyol plus RMN were carried out on a Mettler Toledo Star DSC 821. Samples (4-5 mg) were placed in an aluminum pan and heated up to 120°C under nitrogen atmosphere. In a first heating scan the heating rate was 20°C/min and in all other scans heating and cooling rate of 10°C/min was used. Then samples were cooled -10°C and second heating scan was carried out by heating up to 120 °C at the same heating rates. Moreover in the case of RMN-NLC and the bulk lipid mixture plus RMN the measurements were also performed between 25°-310°C heating range.

RMN content of NLC

The encapsulation efficiency (EE) of RMN and the loading capacity (LC) of NLC were determined by centrifugation followed by dissolution of NLC in methanol, as previously described (28, 29). 100 µl of each NLC batch was loaded in a centrifugal filter (Microcon centrifugal filter unit YM-10 membrane, NMWCO 10 kDa, Sigma Aldrich, St Louis, MO, USA) and centrifuged (Spectrafuge™ 24D Digital Microcentrifuge, Woodbridge NJ, USA) at 8,000 rpm for 20 min. The amount of RMN in the lipid and in the aqueous phase was

determined by high performance liquid chromatography (HPLC), as below reported. The encapsulation parameters were determined as follows.

$$EE = L_{RMN} / T_{RMN} \times 100 \quad (1)$$

$$LC = L_{RMN} / T_{LIPID} \times 100 \quad (2)$$

where L_{RMN} is the amount of drug encapsulated in NLC; T_{RMN} and T_{LIPID} are the total weight of RMN and of lipid used for the NLC preparation, respectively. In the case of NLC produced by "direct method", the amount of RMN was also determined in the OP lost due to: (a) the adhesion (literally, "sticking") between the melted OP and the walls of the glassware and (b) in the floating lipid aggregates present at the surface of the NLC dispersion. In the latest cases, RMN was quantitated by HPLC after dissolution of the collected and weigthed OP in 2 ml of methanol under magnetic stirring.

In vitro release kinetics

In vitro release studies were performed using the dialysis method. Typically, 2 ml of RMN-NLC dispersion was placed into a dialysis tube (6 cm) (molecular weight cut off 10,000-12,000; Medi Cell International, England), then placed into 30 ml of receiving phase constituted of phosphate buffer (100 mM, pH 7.4) and ethanol (70:30, v/v) and shaken in a horizontal shaker (MS1, Minishaker, IKA) at 175 rpm at 37 °C. Samples of receiving phase were withdrawn at regular time intervals, and analyzed by HPLC method as described below. Fresh receiving mixture was added to maintain constant volume. The RMN concentrations were determined four times in independent experiments and the mean values ± standard deviations were calculated.

Drug release data analysis

The experimental release data obtained by the release experiments were fitted to the following semiempirical equations respectively describing Fickian dissolutive and diffusional release mechanisms (30).

$$Mt / M\infty = K_{Diss}\, t^{0.5} + c \qquad (3)$$

$$1 - Mt / M\infty = e^{-Kdiff}\, t + c \qquad (4)$$

where Mt / M∞ is the drug fraction released at the time t, (M∞ is the total drug content of the analyzed amount of NLC), K and c are coefficients calculated by plotting the linear forms of the indicated equations. The release data up to the plateau of percent of released drug were used to produce theoretical release curves.

Animal studies

Male adult Sprague-Dawley rats (320-370 g at the time of the experiments; Charles River Laboratories, Calco, Italy) were housed in groups of two in a temperature-controlled (20±1°C) vivarium and maintained under a 12 h light/dark cycle (07:00 AM-07:00 PM h lights on). Food and water were available *ad libitum*. All experiments were approved by the Italian Ministry of Health (Rome, Italy) and performed in agreement with the guidelines released by the Italian Ministry of Health (D.L. 116/92 and 26/14) and the European Community Directive 2010/63/EU of 22 September 2010. Rats were treated with RMN suspension, RMN-NLC or empty NLC (produced in absence of RMN) and sacrificed 6 hours after administration. ~~In particular each group (n=4) was i.n. administered (200 ul) as following:(a) RMN solution (2.147 mg/ml in PEG 5%, polysorbate 80 5%, saline solution 90%,w/w), (b) RMN-NLC (2.147 mg/ml) or (c) empty NLC.~~ In particular each group (n=4) was i.n. administered (200 ul) as following:(a) RMN solution (2.147 mg/ml in PEG 5%, polysorbate 80 5%, saline solution 90%,w/w), (b) reverse RMN-NLC (2.147 mg/ml) or (c) empty reverse NLC. The dose of RMN for intranasal administration has been selected on

the basis of our own previous studies and literature data. In particular, we administered a dose of the drug that has been proven to antagonize the effects of cannabinoid receptor agonists on different behavioral endpoints, without inducing effects by its own (31-33).

Brain and plasma samples were subjected to a lipid extraction process in accordance with Bhaumik's protocol (34), and the RMN content of the lipid extracts was determined using HPLC as described below. Brains were collected and stored at -80°C until extraction. Before the extraction process, tissues were weighted, diluted with saline solution (1:10 w/v) and homogenized in polypropylene tubes (Sarstedt, Numbrecht, Germany). An aliquot quantity of 0.9 ml plasma sample or homogenized brain was taken in a 10 ml stopper test tube, 8 ml mixed solvent (ethylacetate:n-hexane 70:30, v/v) was then added. Afterwards the mixture was mixed for 15 min and centrifuged at 5000 rpm for 20 min. The organic layer was separated and evaporated to dryness at 40° C under N_2 atmosphere. The residue of all evaporated samples was reconstituted in 300 μl acetonitrile, vortexed for 3 min, and sonicated in 4°C water for 15min. A 50μl aliquot of the clear solution was used for HPLC analysis. All samples were injected in duplicates.

HPLC Procedure

The HPLC apparatus consisted of a two-plungers alternative pump (Jasco, Japan), an UV-detector operating at 260 nm, and a 7125 Rheodyne injection valve. RP-HPLC analysis was performed using a stainless steel C-18 reverse-phase column (15×0.46 cm) packed with 5 μm particles (Grace® - Alltima, Alltech, USA). A pre-column filter Alltima C18 5μm (7.5x0.46 cm) was mounted above the column. Samples of 50 μl were injected through the rheodyne injector system fitted with 50 μl fixed loop. For in vitro studies the elution was performed with a mobile phase containing water and methanol (10:90, v/v) at a flow rate of 0.5 ml/min. Retention time of RMN was 5.0 min. Instead for in vivo experiments, the

mobile phase was constituted of 10 mM phosphate buffer and acetonitrile (30:70, v/v) and the flow rate was 0.5 ml/min. In these conditions the RMN retention time was 16.0 min.

Statistical Analysis

Statistical differences of *in vivo* data were determined using the Student's *t* test. The employed software was Prism 4.0, Graph Pad Software Inc. (La Jolla, CA - USA). P values of less than 0.05 were considered statistically significant.

RESULTS

Preparation of NLC

In order to nano-encapsulate RMN in NLC, a production study was conducted. In particular the step involving the formation of the O/W emulsion has been thoroughly analysed by studying different experimental setup. Notably a weighed amount of RMN in powder form was added at the concentration of 2 mg/ml to the melted lipids (constituting the NLC matrix). After few minutes from the addition of the RMN powder, we observed the complete solubilization of the drug and the formation of an uniform solution.

Regarding the formation of the O/W emulsion, the "direct method", that resulted in the formation a milky dispersion, was characterized by low recovery efficiency; the main loss of lipid phase was due to adhesion phenomena of the lipids to the glassware walls, a further loss was associated to the formation of floating lipid aggregates present at the surface of the NLC dispersion (Table I). The presence of RMN in NLC involved a 6% decrease of both the loss of lipid phase in the beaker and the floating aggregate. It could be supposed that RMN molecule acts in some extent as a surfactant able to stabilize the nanoemulsion, probably placing at the W/O interface. According to this theory RMN should improve nanodroplets generation and then nanoparticles production, preventing in this way the aggregate formation.

To prevent the loss of lipid phase on the walls of the beaker, ascribable to the cooling of the molten lipid phase during its pouring into the vial containing the WP, the use of a reverse modality was proposed. By the reverse method, the loss of lipid phase was indeed limited to the sole presence of a 6% floating aggregate. Moreover the presence of RMN led to a dispersion without aggregates. Taken together these results, on the basis of many studies (35-39), reverse RMN-NLC were treated with polysorbate 80 1% w/w in order to

obtain NLC suitable for targeting to the brain. After polysorbate 80 addition, NLC maintained their milky aspect.

It is to be underlined that the physical stability of NLC (both direct and reverse) was maintained for almost 6 months. Whereas the RMN micellar solution (PEG 5%, polysorbate 80 5%, saline solution 90%, w/w), used as "reference solution", showed drug precipitation after seven days.

Characterization of dispersions

Cryo-TEM

Cryo-TEM analyses were performed with the aim to visualize the structure of NLC within the dispersions.

Figure 1 shows cryo-TEM images of NLC dispersions produced by the direct protocol in absence (1A, 1C) and in presence (1B, 1D) of RMN.

As clearly evident, nanoparticles appear as ovoidal and ellipsoidal platelet-like structures or as dark “needles“ when edge-on viewed (23).

The higher magnification (Fig 1 C and 1D) evidences (a) the inner lamellar morphology of nanoparticles, probably due to tristearin presence, and (b) the caps possibly due to mygliol, resulting in the typical "ufo-like" or "sandwich-like" appearance.

Figure 2 reports images of NLC produced by the reverse protocol in absence (2A, 2C) and in presence of RMN (2B, 2D). In these images one can observe the presence of platelet structures while the inner lamellar morphology is not detectable. In the case of empty NLC no significant differences are appreciable with respect to Figure 1, indicating that production modalities do not affect the NLC aspect.

In Figures 2B and 2D the presence of RMN resulted in more roundish structures with respect to empty NLC, possible suggesting the role of RMN as surfactant agent.

X-ray diffraction measurements

X-ray diffraction was used to investigate the inner structural organization of RMN-NLC. Experiments were performed as a function of temperature on different types of NLC, namely direct and reverse NLC, produced both in absence or in presence of RMN. As a result, very similar X-ray diffraction profiles were obtained, confirming that the inner structure of the NLC is not affected by the presence of RMN or by the production protocol. As an example, Fig. 3 shows the low-angle diffraction observed for RMN-NLC produced by the reverse protocol. In any investigated condition, the observed Bragg peaks indicate that the inner order is lamellar, with a repeat unit cell of 44.2 ± 0.2 Å, as already detected in NLC dispersions used for bromocriptine delivery (40). Finally, Fig. 3 also shows that the diffraction pattern does not depend on the investigated temperature, confirming the strong inner structural stability of such kind of lipid carriers.

PCS analyses

Tables II summarizes the results of PCS studies conducted to determine the dimensional distribution of NLC dispersions. In general all NLC mean diameters were ~200 nm with polydispersity indexes (P.I.) ranging between 0.22 and 0.36. The analyses by intensity, volume and number revealed two populations: the main one with diameter comprised between 84 and 125 nm and the secondary one between 286 and 422 nm.

In particular in the case of NLC produced by the reverse protocol, it can be noted an increase in mean diameters of both populations with respect to direct NLC, analysed by intensity and by volume. PI passed from 0.28 to 0.36.

Analysing dimensional parameters of reverse NLC treated with polysorbate 80, one can observe a mean diameter reduction with respect to untreated reverse NLC. In particular

the analyses by volume and by number reveal a more representative particle population with a mean diameter of ~84 nm.

SdFFF Analysis

NLC size distribution was also determined by SdFFF analysis. The fractograms were converted into PSD plots, as elsewhere described (26, 27).

Figure 4 reports PSD plots of NLC dispersions produced by different protocols. In particular panels A-C report the PSD plots obtained by direct RMN-NLC and reverse RMN-NLC. In Fig. 4A one main peak is followed by a secondary broader peak, indicating two populations of particles: the first one more represented with mean diameter of 82 nm and a second less represented one with a larger diameter (peaking at 170 nm).

In Fig 4B one can observe a negligible first population of particles having a diameter of 70 nm, a broader particle population peaking at 125 nm, whose peak ends with a long tail, which could hide a third population having sizes of about 400 nm, as confirmed by PCS data obtained by intensity and by volume.

SdFFF analysis of reverse RMN-NLC plus polysorbate 80 resulted in a PSD plot analogue to that reported in Fig 4B but lacking of the long tail (data not shown), suggesting that the presence of polysorbate 80 promoted the formation of NLC with smaller mean diameter.

DSC analyses

Figure 5 shows the results of the DSC analysis of NLC (A), RMN-NLC (B) and the bulk mixture of tristearin and miglyol plus RMN (C).

The DSC curve of the bulk mixture of tristearin and miglyol in the absence of the drug is not shown, being superposable to the curve of the bulk lipid mixture in the presence of RMN.

From the DSC thermograms of NLC and RMN-NLC, a double melting point depression peaking at 48.86° and 57.52°C can be noted, due to the melting of lipids. Moreover, only in the case of RMN-NLC, a glass transition (Tg) is observed at 215°C, attributable to the presence of the drug. Instead the Tg was not found nor in NLC, neither in the bulk mixture of lipids plus RMN. In the case of RMN-NLC the Tg presence could suggest that the drug was in amorphous state and homogeneously dispersed within the nanoparticles.

RMN content in NLC

In this study the ultracentrifugation was employed as a method to evaluate RMN content associated to NLC matrix (disperse phase) and in the aqueous phase (dispersing phase).

In the aqueous phase the concentration of RMN was negligible (Table III).

The EE data have been directly obtained evaluating RMN associated to the disperse phase. The reverse protocol led to almost quantitative EE, with a 31.3% increase with respect to the direct protocol (Table III).

It should be noted that only in the case of direct NLC, an amount of RMN was detected also in the lipid phase lost in the beaker and in the floating aggregate.

EE differences between direct RMN-NLC and reverse RMN-NLC were extremely significant.

In vitro release kinetics of RMN from NLC

In order to obtain quantitative and qualitative information on RMN release from NLC, the complete release profile of RMN-NLC was determined in vitro by a dialysis method.

Figure 6A shows that the release kinetic of RMN encapsulated in NLC obtained by reverse protocol and treated with polysorbate 80 was almost linear up to 20 hours, afterwards the amount of RMN released reached a plateau.

RMN release kinetics from direct RMN-NLC (data not shown) were superposable to that from reverse RMN-NLC, indicating that the production protocol doesn't affect the drug release modalities.

Since RMN is scarcely soluble in water, its diffusion kinetic in aqueous physiological receptor phases was undetectable. Therefore a non-physiological receptor phase with 30% v/v of ethanol was used in order to allow the establishment of the sink conditions and to sustain permeant solubilization (41, 42).

The theoretical release curves were determined according to the linear form of Eq.(3) and Eq.(4), mimicking a dissolutive and a diffusive model respectively (40). In Figure 6B the comparison between the theoretical curves calculated from equations (3) and (4) and the experimental curves obtained for NLC are reported. The parameters (K, c and R) determined by linearization of release rate data are reported in the bottom of Figure 6.

The experimental curves reported in Figures 6B are superposable to the theoretical curves calculated from equation (3), referring to dissolutive kinetics.

From the determined values, it is confirmed that RMN release is more consistent with kinetics of the dissolution rather than of the diffusion type, depending on the higher value of R found in the case of linearization of Eq.(3).

Biodistribution studies of RMN-NLC in rats

A preliminary biodistribution study was performed in order to assess the RMN concentration in brain and in plasma 6 hours after i.n. administration. NLC obtained by the WP/OP protocol and treated with polysorbate 80 were employed.

The concentration of RMN in brain and plasma 6h after RMN i.n. administration in rats (n=4) are reported in Table IV and represented by histograms in Figure 7.

The ratio of RMN concentration between brain and plasma ([RMN_{brain}] / [RMN_{plasma}]) was calculated.

In the case of NLC administration, ([RMN_{brain}] / [RMN_{plasma}]) was 17.11, while, in the case of the drug administered by the reference solution, the ratio was 11.74, $p<0.05$.

Discussion

The formulation study enabled to select the protocol for NLC production. Indeed the reverse protocol was chosen since it allowed to prevent loss of lipid phase and consequently to improve EE with respect to the direct protocol.

The nano-encapsulation of RMN allowed to improve its solubility in a stable physiologic aqueous formulation, solving the drawbacks associated with conventional cannabinoid drug administration.

The in vitro release modality of RMN from NLC suggested that the controlling release factor is dissolution rate rather than diffusion rate, as found in another study regarding poor soluble molecules encapsulated in lipid based nanosystems (44).

In vivo data indicate that the concentration of RMN administered by i.n. route was higher in the brain with respect to the plasma and, more importantly, the administration of NLC increased RMN concentration in the brain with respect to the reference solution of RMN.

The i.n. route was chosen since it has been demonstrated to possess a number of advantages (45, 46). In fact drugs administered by this route can bypass the BBB and target the CNS, reducing systemic side effects (47, 48). For this reason delivery may facilitate the treatment and prevention of many different neurologic and psychiatric disorders (49). Finally the i.n. route can be considered as rapid and non-invasive (45, 47).

It is supposed that by i.n. delivery, nanoparticles can bypass the BBB by two ways: the direct olfactory transport and the systemic pathway (50, 51). NLC indeed could be delivered to the central nervous system along both the olfactory and trigeminal nerves pathways or can reach the BBB through systemic circulation (50, 52).

NLC treated with polysorbate 80 were chosen for in vivo studies since it is has been reported that nanoparticles with this surfactant extend circulation time in the blood, decreasing the uptake by the reticulo-endothelial system (53).

Moreover other authors have found that the surfactant would play a specific role in brain targeting, being essential for the delivery of drug-loaded nanoparticles into the brain (35, 36, 54).

It is supposed that polysorbate 80 should be able to inhibit the transporter P-glycoprotein that plays a role in the efflux of a wide range of endogenous and exogenous compounds across biological membranes (55). P-glycoprotein is present also in the apical area of ciliated epithelial cells and in the submucosal vessels of the human olfactory region (49, 56, 57) where it exerts an important role in preventing actively the influx of drugs from nasal membrane.

Thus the impediment of the efflux system in the nasal cavity and in the BBB by polysorbate 80 could enhance the NLC delivery of drugs to the brain.

Nevertheless it should be underlined that at present the mechanism of the inhibition of the P-glycoprotein by polysorbate 80 and the exact process of nanoparticle drug delivery through the BBB have not been explained.

It could be suggested that, after i.n. administration of RMN-NLC, the presence of polysorbate 80 on the solid matrix of nanoparticles could exert an inhibitory effect on the efflux transporter P-glycoprotein, resulting in higher amount of RMN in the brain with respect to the RMN solution.

CONCLUSIONS

The present study demonstrates that a simple adaptation in the production protocol of NLC enables to efficiently nano-encapsulate a cannabinoid drug, obtaining a final stable aqueous physiologic formulation suitable for i.n. administration.

Further studies will be performed in order to investigate kinetics of RMN biodistribution after NLC administration in rats.

Acknowledgements

This work was funded by "FIRB 2010. Fondo per gli Investimenti della Ricerca di Base" from the Ministry of the University and research of Italy. The authors thank Dr. Janne Raula for his help in the interpretation of DSC data.

REFERENCES

1. R.G. Pertwee, Inverse agonism and neutral antagonism at cannabinoid CB1 receptors, Life Sci. 76 (2005) 1307-1324.

2. D.R. Janero, A. Makriyannis, Cannabinoid receptor antagonists: pharmacological opportunities, clinical experience, and translational prognosis, Expert. Opin. Emerg. Drugs 14 (2009) 43-65.

3. P. Pacher, S. Batkai, G. Kunos, The endocannabinoid system as an emerging target of pharmacotherapy, Pharmacol. Rev. 58 (2006) 389-462.

4. K. Mackie, Cannabinoid receptors as therapeutic targets, Annu. Rev. Pharmacol. Toxicol. 46 (2006) 101-122.

5. V. Trezza, P. Campolongo, The endocannabinoid system as a possible target to treat both the cognitive and emotional features of post-traumatic stress disorder (PTSD), Front. Behav. Neurosci. 7 (2013) 1-5.

6. M. Morena, P. Campolongo, The endocannabinoid system: An emotional buffer in the modulation of memory function, Neurobiol. Learn Mem. (2013) pii: S1074-7427(13)00266-9. doi: 10.1016/j.nlm.2013.12.010. [Epub ahead of print]

7. P. Campolongo, M. Morena, S. Scaccianoce, V. Trezza, F. Chiarotti, G. Schelling, V. Cuomo, B. Roozendaal, Novelty-induced emotional arousal modulates cannabinoid effects on recognition memory and adrenocortical activity, Neuropsychopharmacology. 38 (2013) 1276-1286.

8. V. Trezza, R. Damsteegt, A. Manduca, S. Petrosino, L.W. Van Kerkhof, R.J. Pasterkamp, Y. Zhou, P. Campolongo, V. Cuomo, V. Di Marzo, L.J. Vanderschuren, Endocannabinoids in amygdala and nucleus accumbens mediate social play reward in adolescent rats, J Neurosci. 32 (2012) 14899-14908.

9. P. Pacher, G. Kunos, Modulating the endocannabinoid system in human health and disease--successes and failures, FEBS J. 280 (2013) 1918-1943.

10. R.G. Pertwee, Targeting the endocannabinoid system with cannabinoid receptor agonists: pharmacological strategies and therapeutic possibilities, Philos. Trans. R. Soc. Lond. B Biol. Sci. 367 (2012) 3353-3363.

11. D.H. Pérez de la Ossa, A. Ligresti, M.E. Gil-Alegre, M.R. Aberturas, J. Molpeceres, V. Di Marzo, A. Torres Suárez, Poly-ε-caprolactone microspheres as a drug delivery system for cannabinoid administration: development, characterization and in vitro evaluation of their antitumoral efficacy, J. Contro.l Release. 161 (2012) 927-32.

12. L. Battaglia, M. Gallarate, Lipid nanoparticles: state of the art, new preparation methods and challenges in drug delivery, Expert Opin. Drug Deliv. 9 (2012) 497-508.

13. A.M. Nyström, B. Fadeel, Safety assessment of nanomaterials: Implications for nanomedicine, J. Control. Release 16 (2012) 403-408.

14. M. Uner, G. Yener, Importance of solid lipid nanoparticles (SLN) in various administration routes and future perspectives, Int. J. Nanomedicine 2 (2007) 289-300.

15. M.D. Joshi, R.H. Müller, Lipid nanoparticles for parenteral delivery of actives, Europ. J. Pharm. Biopharm. 71 (2009) 161-172.

16. A. Saupe, S.A. Wissing, A. Lenk, C. Schmidt, R.H. Müller, Solid lipid nanoparticles (SLN) and nanostructured lipid carriers (NLC) - structural investigations on two different carrier systems, Biomed. Mater. Eng. 15 (2005) 393-402.

17. G. Yoon, J.W. Park, I.-S. Yoon, Solid lipid nanoparticles (SLNs) and nanostructured lipid carriers (NLCs): recent advances in drug delivery, J. Pharm. Investig. 43 (2013) 353-362.

18. S.S. Shidhaye, R. Vaidya, S. Sutar, A. Patwardhan, V.J. Kadam, Solid lipid nanoparticles and nanostructured lipid carriers--innovative generations of solid lipid carriers, Curr. Drug Deliv. 5 (2008) 324-31.

19. A. Puri, K. Loomis, B. Smith, J.H. Lee, A. Yavlovich, E. Heldman, R. Blumenthal, Lipid-based nanoparticles as pharmaceutical drug carriers: from concepts to clinic, Crit. Rev. Ther. Drug Carrier Syst. 26 (2009) 523-80.

20. R. Christensen, P.K. Kristensen, E.M. Bartels, H. Bliddal, A. Astrup, Efficacy and safety of the weight-loss drug rimonabant: a meta-analysis of randomised trials, Lancet 370 (2007) 1706-1713.

21. K. Johansson, K. Neovius, S.M. DeSantis, S. Rössner, M. Neovius, Discontinuation due to adverse events in randomized trials of orlistat, sibutramine and rimonabant: a meta-analysis, Obes. Rev. 10 (2009) 564-575.

22. K. Jores, W. Mehnert, M. Drechsler, H. Bunjes, C. Johann, K. Maeder, Investigations on the structure of solid lipid nanoparticles (SLN) and oil-loaded solid lipid nanoparticles by photon correlation spectroscopy, field-flow fractionation and transmission electron microscopy, J. Control. Release 95 (2004) 217-227.

23. E. Esposito, M. Fantin, M. Marti, M. Drechsler, L. Paccamiccio, P. Mariani, E. Sivieri, F. Lain, E. Menegatti, M. Morari, R. Cortesi, Solid lipid nanoparticles as delivery systems for bromocriptine, Pharm. Res. 25 (2008) 1521-1530.

24. V. Luzzati, H. Delacroix, T. Gulik-Krzywicki, P. Mariani, R. Vargas, The cubic phases of lipids, Curr. Top. Membr. 44 (1997) 3-24.

25. R. Pecora, Dynamic Light Scattering Measurement of Nanometer Particles in Liquids, J. Nanoparticle Res. 2 (2000) 123-131.

26. C. Contado, A. Dalpiaz, E. Leo, M. Zborowski, P.S. Williams, Complementary use of flow and sedimentation field-flow fractionation techniques for size characterizing biodegradable poly(lactic acid) nanospheres, J. Chromatogr. A 1157 (2007) 321-335.

27. C. Contado, G. Blo, F. Fagioli, F. Dondi, R. Beckett, Characterisation of River Po particles by sedimentation field-flow fractionation coupled to GFAAS and ICP-MS, Colloid Surface A 120 (1997) 47-59.

28. A.P. Nayak, W. Tiyaboonchai, S. Patankar, B. Madhusudhan, E.B. Souto, Curcuminoids loaded lipid nanoparticles: Novel approach towards malaria treatment, Colloid Surface B 81 (2010) 263-273.

29. C. Puglia, V. Cardile, A.M. Panico, L. Crascì, A. Offerta, S. Caggia, M. Drechsler, P. Mariani, R. Cortesi, E. Esposito, Evaluation of monooleine aqueous dispersions as tools for topical administration of curcumin: characterization, in vitro and ex-vivo studies, J. Pharm. Sci. 102 (2013) 2349–2361.

30. E. Esposito, E. Menegatti, R. Cortesi, Hyaluronan based microspheres as tools for drug delivery: a comparative study, Int. J. Pharm. 288 (2005) 35–49.

31. B. Bosier, S. Sarre, I. Smolders, Y. Michotte, E. Hermans, D.M. Lambert, Revisiting the complex influences of cannabinoids on motor functions unravels pharmacodinamic differences between cannabinoid agonists, Neuropharmacol. 59 (2010) 503-510.

32. M. Bortolato, P. Campolongo, R.A. Mangieri, M.L. Scattoni, R. Frau, V. Trezza, G. La Rana, R. Russo, A. Calignano, G.L. Gessa, V. Cuomo, D. Pionelli, Anxiolytic-like properties of the anandamide transport inhibitor AM404, Neuropsychopharmacol. 31 (2006) 2652-2659.

33. P. Campolongo, V. Trezza, P. Ratano, M. Palmery, V. Cuomo, Developmental consequences of perinatal cannabis exposure: behavioral and neuroendocrine effects in adult rodents, Psychopharmacology (Berl). 214 (2011) 5-15.

34. U. Bhaumik, A. Ghosh, B. Chatterjee, P. Sengupta, S. Darbar, B. Roy, U. Nandi, TK. Pal, Development and validation of a high-performance liquid chromatographic method for bioanalytical application with rimonabant, J. Pharm. Biomed. Anal. 49 (2009) 1009-1013.

35. J. Kreuter, V.E. Petrov, D.A. Kharkevich, R.N. Alyautdin, Influence of the type of surfactant on the analgesic effects induced by the peptide dalargin after its delivery across the blood -brain barrier using surfactant-coated nanoparticles, J. Control. Release 49 (1997) 81-87.

36. P. Ramge, R.E. Unger, B. Oltrogge, D. Zenker, D. Begley, J. Kreuter, H. von Briesen, Polysorbate-80 coating enhances uptake of polybutylcyanoacrylate (PBCA) nanoparticles by human and bovine primary brain capillary endothelial cells, Eur J Neurosci. 12 (2000) 1931 -1940.

37. A.E. Gulyaev, S.E. Gelperina, I.N. Skidan, A.S. Antropov, G.Y. Kivman, J. Kreuter, Significant transport of doxorubicin into the brain with polysorbate 80-coated nanoparticles, Pharm. Res. 16 (1999) 1564-1569.

38. T.M. Göppert, R.H. Müller, Polysorbate-stabilized solid lipid nanoparticles as colloidal carriers for intravenous targeting of drugs to the brain: comparison of plasma protein adsorption patterns. J. Drug Target. 13 (2005) 179-187.

39. X.H. Tian, X.N. Lin, F. Wei, Z.C. Huang, P. Wang, L. Ren, Y. Diao, Enhanced brain targeting of temozolomide in polysorbate-80 coated polybutylcyanoacrylate nanoparticles, Int. J. Nanomed. 6 (2011) 445-452.

40. E. Esposito, P. Mariani, L. Ravani, C. Contado, M. Volta, S. Bido, M. Drechsler, S. Mazzoni, E. Menegatti, M. Morari, R. Cortesi, Nanoparticulate lipid dispersions for bromocriptine delivery: characterization and in vivo study, Eur. J. Pharm. Biopharm. 80 (2012) 306-314.

41. M. Siewert, J. Dressman, C.K. Brown, V.P. Shah, FIP/AAPS guidelines to dissolution/in vitro release testing of novel/special dosage forms, AAPS PharmSciTech 4 (2003) E7.

42. E. Toitou, B. Fabin, Altered skin permeation of highly lipophilic molecule: tetrahydrocannabinol, Int. J. Pharm. 43 (1988) 17-22.

43. N.A. Peppas, Analysis of Fickian and non-Fickian drug release from polymers, Pharm. Acta Helv. 60 (1985) 110-111

44. J. Lee, I.W. Kellaway, The controlled release of drugs from cubic phases of glyceryl monooleate, in: M.L. Lynch, P.T. Spicer (Eds.), Bicontinuous Liquid Crystals, CRC Press, Taylor & Francis Group, Boca Raton (FL), 2005, pp. 457-469.

45. L. Illum, Nasal drug delivery – possibilities, problems and solutions. J. Control. Release 87 (2003) 187- 198.

46. C.L. Graff, G.M. Pollack, Nasal drug administration: potential for targeted central nervous system delivery, J. Pharm. Sci. 94 (2005) 1187-1195.

47. H.R. Costantino, L. Illum, G. Brandt, P.H. Johnson, SC. Quay, Intranasal delivery: physicochemical and therapeutic aspects, Int. J. Pharm. 337 (2007) 1-24.

48. S.V. Dhuria, L.R. Hanson, W.H. Frey, Intranasal delivery to the central nervous system: mechanisms and experimental considerations, J. Pharm. Sci. 99 (2010) 1654-1673.

49. A. Pires, A. Fortuna, G. Alves, A. Falcão, Intranasal drug delivery: how, why and what for? J. Pharm. Pharmaceut. Sci. 12 (2009) 288-311.

50. L. Illum, Transport of drugs from the nasal cavity to the central nervous system, Eur. J. Pharm. Sci. 11 (2000) 1-18.

51. Q.-Z. Zhang, L.-S. Zha, Y. Zhang, W.-M. Jiang, W. Lu, Z.-Q. Shi, X.-G. Jiang, S.-K. Fu, The brain targeting efficiency following nasally applied MPEG-PLA nanoparticles in rats, J. Drug Target. 14 (2006) 281-290.

52. H. Yang, Nanoparticle-mediated brain-specific drug delivery, imaging, and diagnosis, Pharm. Res. 27 (2010) 1759-1771.

53. A. Ambruosi, H. Yamamoto, J. Kreuter, Body distribution of polysorbate-80 and doxorubicin-loaded [^{14}C]poly(butyl cyanoacrylate) nanoparticles after i.v. administration in rats, J. Drug Target. 13 (2005) 535-542.

54. Y. Ruan, L. Yao, B. Zhang, S. Zhang, J. Guo, Antinociceptive properties of nasal delivery of neurotoxin-loaded nanoparticles coated with polysorbate-80, Peptides 32 (2011) 1526-1529.

55. ML. Amin, P-glycoprotein inhibition for optimal drug delivery, Drug Target Insights. 7 (2013) 27-34.

56. C.L. Graff, G.M. Pollack, Functional evidence for P-glycoprotein at the nose-brain barrier, Pharm. Res. 22 (2005) 86-93.

57. U. Westin, E. Piras, B. Jansson, U. Bergström, M. Dahlin, E. Brittebo, E. Björk, Transfer of morphine along the olfactory pathway to the central nervous system after nasal administration to rodents, Eur. J. Pharm. Sci. 24 (2005) 565-573.

LEGENDS TO FIGURES

Figure 1. Cryo-transmission electron microscopy images (cryo-TEM) of NLC samples produced by the direct protocol. A, C: empty NLC, B, D: RMN-NLC.

Figure 2. Cryo-TEM images of NLC samples produced by the reverse protocol. A, C: empty NLC, B, D: RMN-NLC.

Figure 3. X-ray diffraction profiles for NLC samples produced by the reverse protocol in absence (empty NLC) and in presence of RMN (RMN-NLC). In the last case, profiles observed at different temperatures (37 and 45°C) are reported. The dotted lines indicate the position of the (100) and (200) lamellar Bragg peaks

Figure 4. PSD plots of RMN-NLC obtained by the direct method (A) and RMN-NLC obtained by the reverse method (B).

Figure 5. DSC analysis of NLC (A) and RMN-NLC (B) and the bulk mixture of tristearin and mygliol plus RMN (C).

Figure 6. (A) In vitro release kinetics of RMN encapsulated in NLC obtained by the reverse protocol plus polysorbate 80. Experiments were performed by dialysis method. Data were the mean of 4 experiments.

(B) Comparison of the theoretical (dotted lines) and experimental (●, solid lines) RMN profiles from NLC. The theoretical curves were obtained using the coefficient calculated by linear regression of the linearized form of equation (3) (crosses) and equation (4) (circles). The bottom frame reports the kinetic parameters of RMN release from reverse NLC.

Figure 7. RMN concentration in brain (b) and in plasma (p) 6 h after intranasal administration of RMN by reverse NLC (RMN-NLC) or by solution (RMN-sol) in rats. Error bars represent the standard deviations, n=4, *$p<0.05$ by paired Student's *t* test.

Figure 1

Click here to download high resolution image

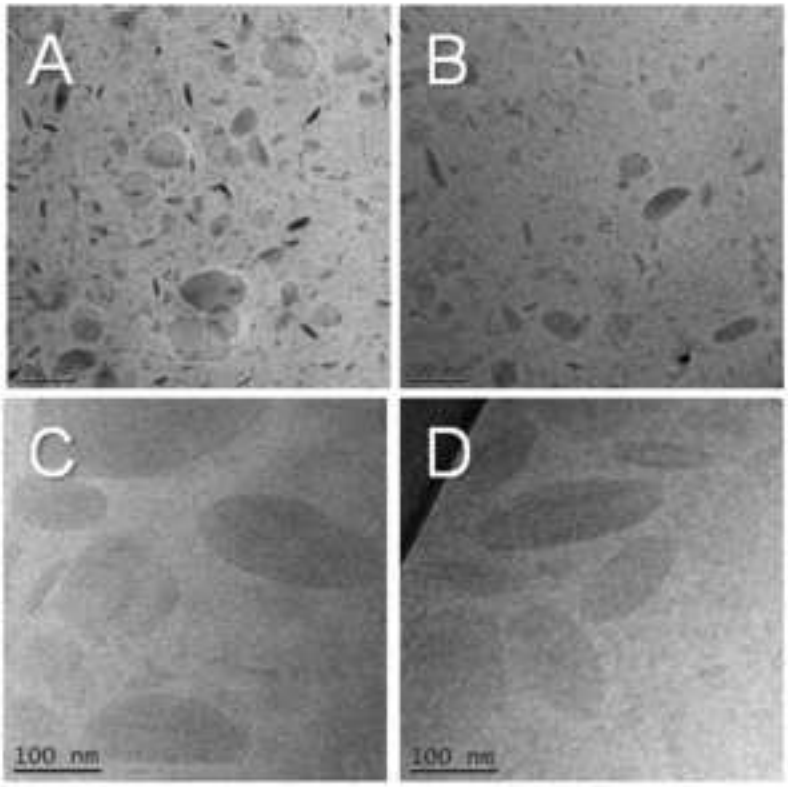

Figure 1

Figure 2

Click here to download high resolution image

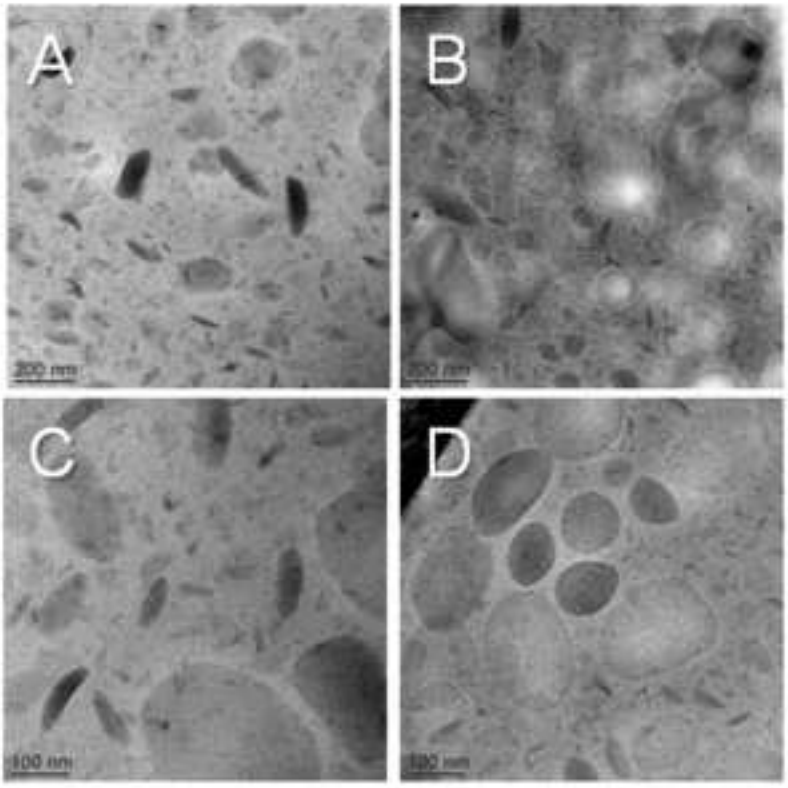

Figure 2

Figure 3

Click here to download high resolution image

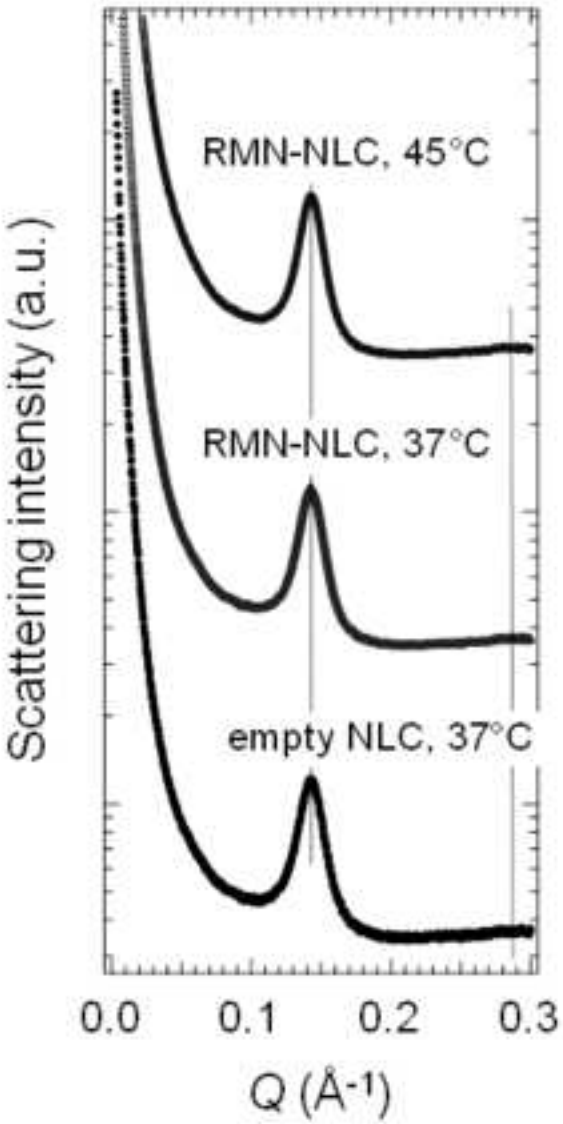

Figure 3

Figure 4

Click here to download high resolution image

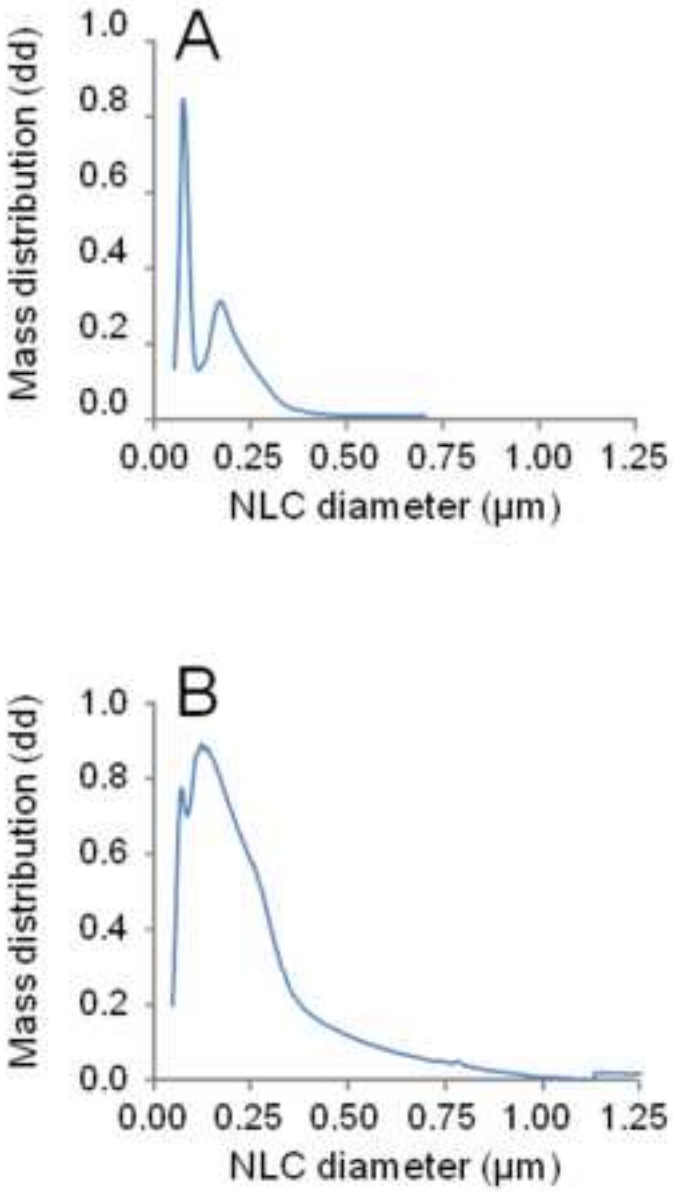

Figure 4

Figure 5

Click here to download high resolution image

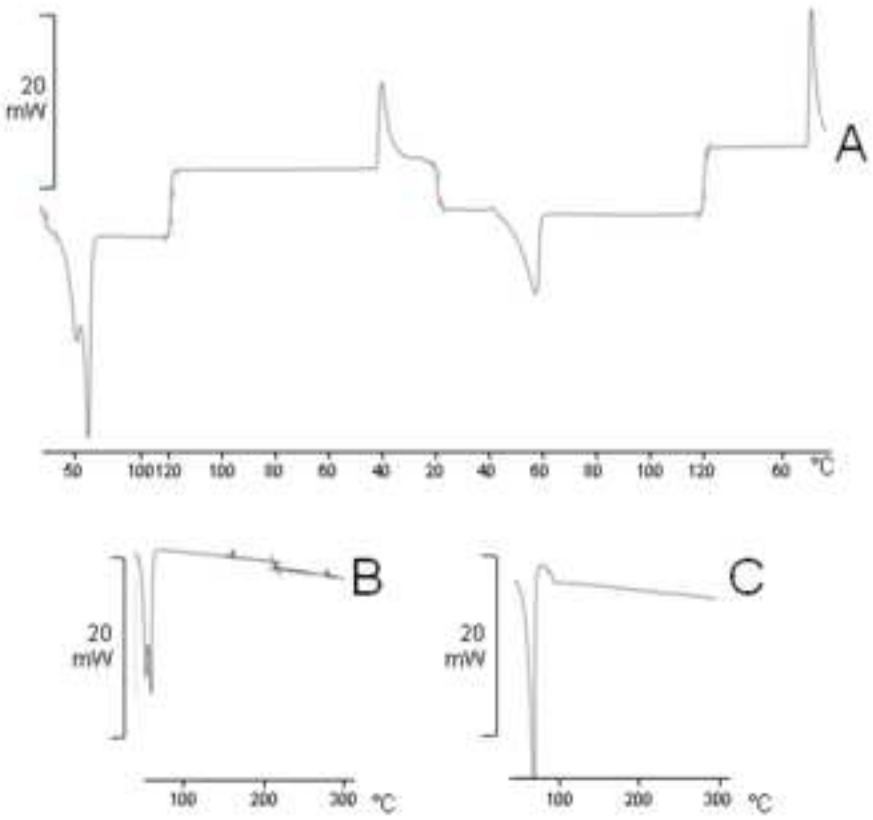

Figure 5

Figure 6

Click here to download high resolution image

A

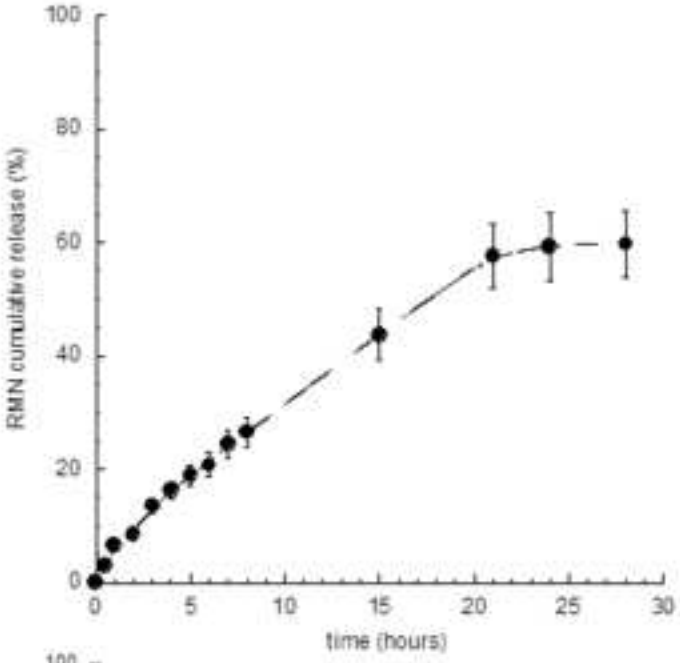

B

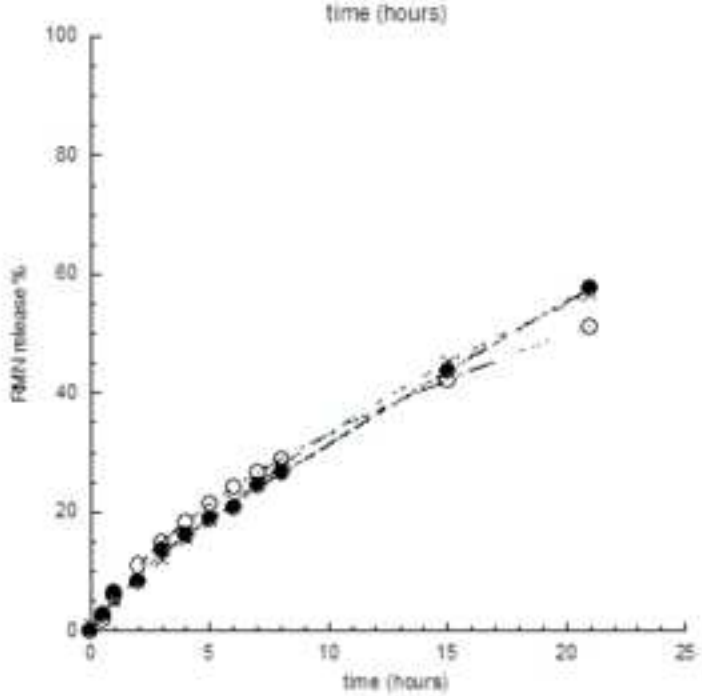

Kinetic parameters of RMN release from reverse NLC

Equation	K	c	R
$Mt/M\infty = K_{Diff}t^{0.5} + c$	-0.039255	4.5947	0.99817
$1 - Mt/M\infty = e - K_{Diff}t + c$	12.691	-6.9689	0.97807

Figure 6

Figure 7

Click here to download high resolution image

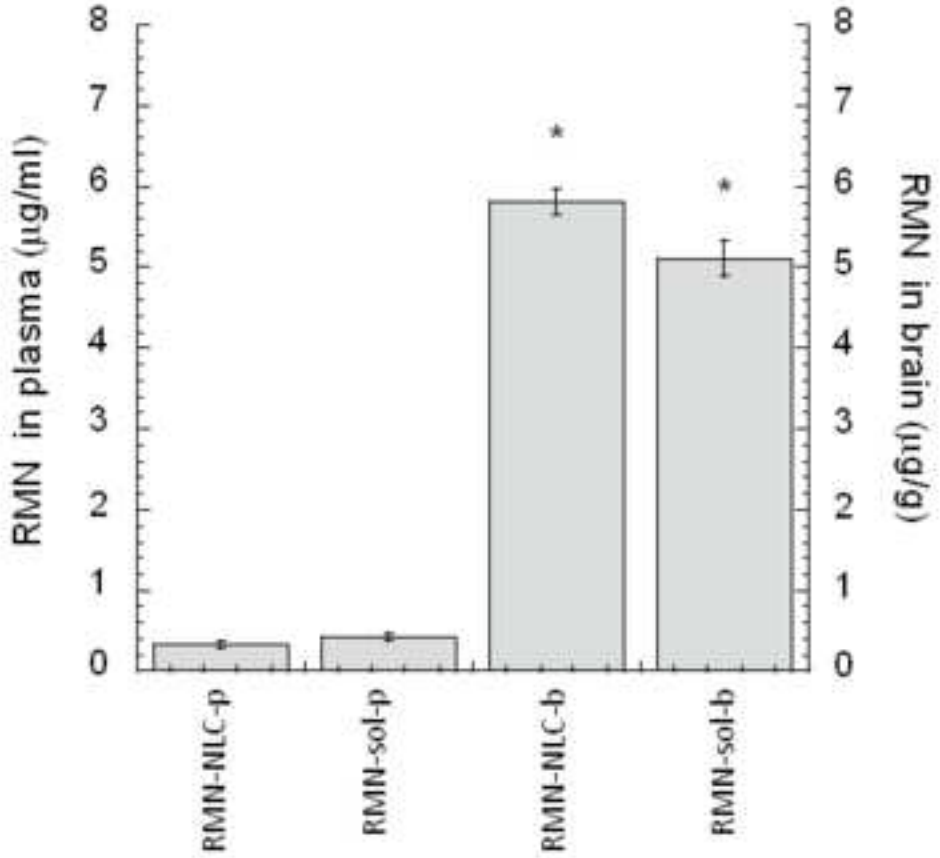

Figure 7

Table

Table I Effect of preparation method on the recovery of NLC

	preparation procedure			
	"direct method"		"reverse method"	
	empty NLC	RMN-NLC	empty NLC	RMN-NLC
% recovery	73.1	75.8	93.7	92.5
loss due to adhesion[a]	20.5 (0.5)	14.1 (0.2)	n.d.	n.d.
loss due to coalescence[b]	16.4 (0.1)	10.1 (0.3)	6.3 (0.3)	7.5

Percent of recovery was calculated as follows:

% recovery = amount of NLC recovered (g) / amount of lipid used (g) x 100.

Data represent the mean ± SD (reported in parentheses) of 6 independent experiments-
[a]Loss of lipids (OP) due to the adhesion (literally, "sticking") between the melted OP and the walls of the glassware employed for its melting and pouring into the WP.
[b]Loss of lipids (OP) due to the partial coalescence of the OP during the formation of the O/W emulsion. After cooling the coalesced OP appeared as a small flake floating on the surface of the NLC dispersion. n.d. = not detectable.

Table II: Dimensional characteristics of the produced NLC

	"direct method"	"reverse method"	
	RMN-NLC	RMN-NLC	RMN-NLC + polysorbate 80
Z average (nm)	206	204	204
Mean diameter by intensity (nm)	98 (48%) 295 (52%)	126 (71%) 377 (29%)	85 (44%) 356 (56%)
Mean diameter by volume (nm)	95 (76%) 335 (24%)	106 (63%) 422 (37%)	85 (86%) 286 (14%)
Mean diameter by number (nm)	93	92	84

Table III: Encapsulation efficiency of RMN in NLC

Formulation	RMN distribution (% of T_{RMN})			
	in NLC	in lipids sticking to the glassware	in the floating lipid aggregate	In the dispersing phase
"direct method"	67 ± 1.3	13 ± 1.4	18 ± 0.4	2 ± 0.2
"reverse method"	98 ± 0.4	n.d.	n.d.	2 ± 0.2

T_{RMN} is the total weight of RMN used for the NLC preparation,
n = 6, $p<0.0001$ by paired Student's t test. n.d. = not detectable.

Table IV: Plasma and brain distributions of RMN after intranasal administration

Formulation	Plasma (ng/ml)	Brain (μg/g)
RMN-NLC°	340.2 ± 33.7	5.8 ± 0.2
RMN-sol*	435.1 ± 42.2	5.1 ± 0.2

°RMN encapsulated in NLC + polysorbate 80 produced by the "reverse method"
*RMN solubilized in saline/PEG/ polysorbate 80 (90:5:5, v/v/v)
Data represent the average of the determinations carried on 4 animals, $p<0.05$ by paired Student's t test.